

Direct velocity measurements of the flow past drag-reducing ultrahydrophobic surfaces

Jia Ou and Jonathan P. Rothstein

Department of Mechanical and Industrial Engineering, University of Massachusetts, Amherst, Massachusetts 01003-2210

(Received 7 April 2005; accepted 14 September 2005; published online 20 October 2005)

A series of experiments are presented which study the flow kinematics of water past drag-reducing superhydrophobic surfaces. The ultrahydrophobic surfaces are fabricated from silicon wafers using photolithography and are designed to incorporate precise patterns of micrometer-sized ridges aligned in the flow direction. The ridges are made hydrophobic through a chemical reaction with an organosilane. An experimental flow cell is used to measure the velocity profile and the pressure drop as a function of the flow rate for a series of rectangular cross-section microchannel geometries and ultrahydrophobic surface designs. The velocity profile across the microchannel is determined through microparticle image velocimetry (μ -PIV) measurements capable of resolving the flow down to lengthscales well below the size of the surface features. Through these detailed velocity measurements, it is demonstrated that slip along the shear-free air-water interface supported between the hydrophobic micrometer-sized ridges is the primary mechanism responsible for the drag reduction observed for flows over ultrahydrophobic surfaces. A maximum slip velocity of more than 60% of the average velocity in the microchannel is found at the center of the shear-free air-water interface whereas the no-slip boundary condition is found to hold along the surface of the hydrophobic ridges. The experimental velocity and pressure drop measurements are compared to the predictions of numerical simulations and an analytical theory based on a simple model of an ultrahydrophobic surface composed of alternating shear-free and no-slip bands with good agreement. © 2005 American Institute of Physics. [DOI: 10.1063/1.2109867]

I. INTRODUCTION

In devices where the fluid flow is laminar and not turbulent, there are currently few demonstrated methods for significantly reducing drag. The development and understanding of such a technology could have a significant impact as mechanical technology is miniaturized, microfluidic devices become more widely used, and biomedical analysis moves aggressively towards lab on a chip technologies. In this manuscript, through a carefully designed set of experiments we will study the detailed kinematics of the flow through microchannels having walls fabricated from hydrophobic surfaces with well-defined micrometer-sized roughness. Through these measurements and the results of numerical simulations, we will verify the physical origins of drag reduction in flows past ultrahydrophobic surfaces.

Originally inspired by the unique water repellent properties of the lotus leaf,¹ ultrahydrophobic surfaces have recently been developed which are capable of obtaining contact angles that approach $\theta=180^\circ$.²⁻⁷ The difference between a hydrophobic surface and an ultrahydrophobic surface lies not in the surface chemistry, but in the microscale surface roughness. Ultrahydrophobic surfaces are rough with micrometer-sized protrusions coming out of the surface. The hydrophobicity of the microscale surface roughness prevents the water from moving into the pores between the peaks of the microposts. Instead of wetting the entire surface, the water stands off, touching only the peaks of the surface roughness and resulting in the air-water interface seen schemati-

cally in Fig. 1. The result is the near elimination of the contact angle hysteresis and a dramatic reduction of the resistance to drop motion.^{3,6,8} For a more complete review of relevant literature on ultrahydrophobic surfaces and drag reduction, the reader is referred to our previous publication.⁹ For the sake of brevity, a detailed review will only be provided for the most relevant publications.

Ou *et al.*⁹ demonstrated that the same physical mechanism that produced drag reduction in the motion of drops on ultrahydrophobic surfaces could also produce drag reduction in flows without contact lines. Using lithographically etched silanized silicon surfaces with precisely controlled microsurface topology consisting of regular arrays of microposts and microridges, they systematically investigated the affect of topological changes on drag reduction.⁹ At the microchannel lengthscales investigated in their experiments, the boundary condition for the fluid in contact with the top of the micropost or microridge is no-slip, however, the air-water interfaces supported between microposts or microridges is shear-free, essentially providing no resistance to the flow. Ou *et al.*⁹ demonstrated the existence and subsequent deflection of the air-water interface under flow through laser confocal surface metrology measurements of the interface. Pressure drop reductions in excess of $\Pi=(\Delta p_{\text{no-slip}}-\Delta p)/\Delta p_{\text{no-slip}}>35\%$ and slip lengths greater than $b>20\ \mu\text{m}$ were achieved through a reduction of the effective surface area of the solid in contact with the flowing fluid.⁹ Here Δp is the experimentally measured pressure drop and $\Delta p_{\text{no-slip}}$ is the pressure drop measured for flow over a no-slip surface at the same

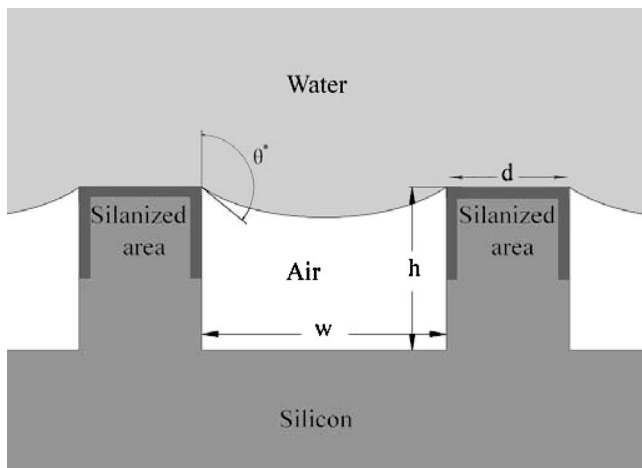


FIG. 1. Schematic diagram of a model for ultrahydrophobic drag reduction. A combination of surface hydrophobicity and roughness combine to allow water to stand off from the solid surface.

flow rate. Ou *et al.* demonstrated that by either decreasing the size of the microposts or microridges and/or increasing the separation between them resulted in a reduction in the flow resistance and the generation of significant drag reduction.⁹

Because the surface topology of the photolithographically etched silicon surface could be precisely designed and controlled, Ou *et al.*⁹ were able to compare the results of their drag reduction measurements directly to the analytical solutions of Philip^{10,11} and Lauga and Stone.¹² Philip analytically solved the Stokes flow problem for flow in an infinite channel where one wall is no-slip whereas the other wall contains a shear-free band running parallel to the flow direction.^{10,11} The experimental pressure drop reduction measurements were found to agree qualitatively with the predictions of the analytical solution, however, the analytical solution was found to systematically underpredict the magnitude of the pressure drop reduction.⁹

The presence of drag reduction is often macroscopically modeled as a slip velocity at the wall surface. In Navier's model, the slip velocity at the wall, $u_{x,0}$, is defined to be proportional to the shear rate experienced by the fluid at the wall, $u_{z,0} = b(\partial u_z / \partial y)$, where b is the slip length.¹³ For the flow of simple fluids flowing past hydrophobic smooth surfaces a number of studies have calculated slip lengths indirectly from pressure drop or friction factor measurements.^{14–18} For the flow between two infinite parallel plates where the slip length is large, the slip length can be calculated from measurements of the volume flow rate per unit length, q , and the pressure gradient, dp/dx

$$q = \frac{H^3}{4\mu} \left(-\frac{dp}{dz} \right) \left[\frac{1}{3} + \frac{b}{b+H} \right]. \quad (1)$$

Here H is the distance between the plates and μ is the viscosity of the fluid.

However, because the slip lengths and therefore the slip velocities for the flow over smooth hydrophobic surfaces are typically small, $b \ll 100$ nm, only a few direct measurements of the slip velocity at or near the wall have been made.^{19–23}

Using microparticle image velocimetry (μ -PIV) measurements, Tretheway and Meinhardt^{19,20} found a relatively large slip velocity for the flow of water through a microchannel where the walls were coated with a monolayer of hydrophobic octadecyltrichlorosilane. Pit *et al.*²¹ used total internal reflection fluorescence recovery after photobleaching to measure a slip velocity of hexadecane flowing past a lyophobicity modified smooth sapphire surface. The use of total internal reflection fluorescence microscopy allowed Pit *et al.*²¹ to probe the fluid velocity in close proximity (<100 nm) of the solid surface. Very recently Jin *et al.*²² combined evanescent wave illumination of submicrometer particles with particle tracking velocimetry to measure the slip velocity of water near a glass surface coated with a self-assembled monolayer of octadecyltrichlorosilane. Using this total internal reflection velocimetry technique Jin *et al.*²² were able to resolve small slip velocities from measurements very close to the hydrophobic surface.

Direct velocity measurements have also been made for flow past ultrahydrophobic surfaces. Watanabe *et al.*^{24,25} investigated the flow of water through 6 and 12 mm diameter circular pipes having a highly water repellent walls. The walls of the pipes were coated with a fluorine alkane modified acrylic resin resulting in a porous hydrophobic surface crisscrossed by 10–20 μ m wide microcracks to form an ultrahydrophobic surface. Velocity profiles in the pipe were measured through hot-film anemometry. Slip velocities greater than $u_{z,0} > 2$ cm/s and slip lengths greater than $b > 450$ nm were found for flows with Reynolds numbers between $500 < \text{Re} < 10\,000$.^{24,25} However, because the patterns of microcracks on the pipe walls were randomly spaced and oriented and the resolution of the hot-wire anemometry technique was large compared to the scale of the microcracks, the velocity profile and slip velocity measurements of Watanabe *et al.*^{24,25} represent average values of the flow. The detailed kinematics of the flow near the ultrahydrophobic surface and the interactions between the water and the free surface that may exist at or near the microcracks cannot be determined from their measurements, thus making a more complete understanding of their drag reduction mechanism difficult.

In the experiments that are described in this manuscript, photolithographically etched silanized silicon surfaces are used to precisely control the microsurface topology thereby allowing us to systematically and precisely probe the detailed flow kinematics throughout the microchannel. Using μ -PIV, measurements are made above both the microridges and the air-water interface supported between the microridges. These measurements are then compared to the predictions of a series of three-dimensional numerical simulations and an analytical theory for the Stokes flow past a periodic array of microridges aligned in the flow directions. The results provide further proof that ultrahydrophobic drag reduction is due to the existence of a shear-free air-water interface between microperturbations resulting in a reduced effective contact area between the fluid and the solid surface.

The outline of this paper is as follows. In Sec. II, we describe the experimental setup, fabrication of the ultrahydrophobic surfaces and numerical simulations. In Sec. III, we

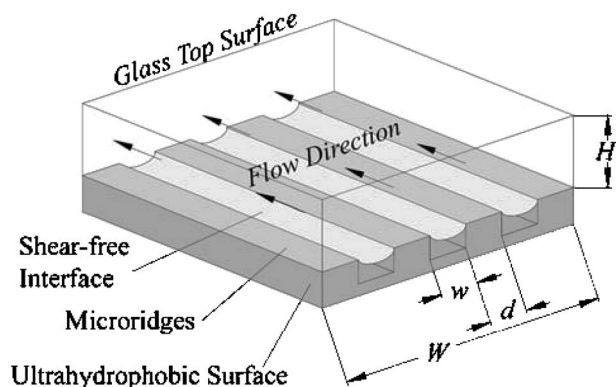


FIG. 2. Schematic diagram of the experimental microchannel flow cell including the important physical dimensions.

present and compare our experimental velocity and pressure drop measurement to the predictions of our numerical simulation. Finally, in Sec. IV we conclude.

II. EXPERIMENT

A. General procedures

The experimental flow cell shown in Fig. 2 was designed and fabricated to measure the pressure drop resulting from the laminar flow of water through a rectangular microchannel. A series of rectangular cross section microchannels with a thickness between $76 \mu\text{m} < H < 254 \mu\text{m}$ were precisely machined from plastic. As the thickness of the microchannels was changed, the aspect ratio of each microchannel and the overall length of the microchannel were held fixed at $\alpha = W/H = 20$ and $L = 50 \text{ mm}$, respectively. A smooth hydrophilic piece of glass was used as the upper wall of the microchannel to allow for optical access to the flow. The lower wall of the flow cell was designed to be easily interchangeable making it possible to perform drag reduction and μ -PIV measurements on a host of different surfaces including a series of ultrahydrophobic silicon wafers with a prescribed surface roughness pattern and smooth hydrophobic silicon wafers. For a more complete description of the flow cell, the reader is referred to Ou *et al.*⁹

An inlet and outlet were machined into the glass cover slip. A syringe pump (Model 100, KD Scientific Inc., Massachusetts, USA) was used to drive the fluid through the microchannel with flow rates between 0.03 and 115 mm^3/s . The pressure drop was measured using a manometer with a resolution of 0.25 mm water height or equivalently 2.5 Pa. For all of the experimental measurements reported in the following sections, the Reynolds number based on the hydraulic diameter was less than $\text{Re} < 1000$ and thus the flows were all laminar.²⁶ Here the Reynolds number is defined as $\text{Re} = \rho U D_H / \mu$, where ρ is the density of the fluid, $U = Q/A$ is the average velocity, Q is the volume flow rate, A is the cross sectional area of the channel, $D_H = 4A/P$ is the hydraulic diameter and P is the perimeter of the channel.

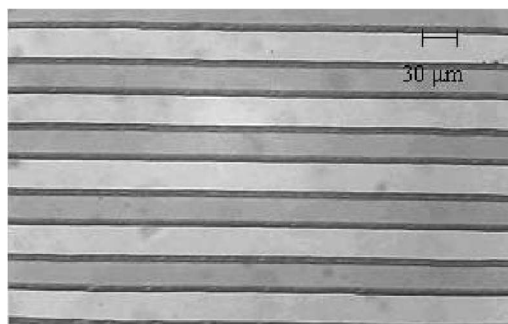


FIG. 3. Micrographs of ultrahydrophobic surface with microridges etched onto a silicon wafer.

B. Preparation of ultrahydrophobic silicon surfaces

In order to fabricate the ultrahydrophobic surfaces, standard photolithographic techniques were used to precisely and reproducibly control the size, height, spacing and geometry of the micrometer scale roughness designed onto silicon wafers.^{9,27} Once the desired roughness was imparted on the silicon wafer, it was reacted with a silanizing agent to make it ultrahydrophobic.^{2,9} For details of the fabrication procedure used to make the ultrahydrophobic surfaces used in the experiments that follow, the reader is referred to our previous publication.⁹ An image from an optical microscope of one of the ultrahydrophobic surfaces used in these experiments is shown in Fig. 3. The advancing and receding contact angles of a droplet on the ultrahydrophobic surface in Fig. 3 was measured to be $162^\circ/137^\circ$. These values are typical for the surfaces used throughout our experiments. For comparison, the advancing receding contact angle for a hydrophobic smooth silicon surface was measured to be $118^\circ/100^\circ$.

The ultrahydrophobic surfaces were patterned with both $d = 20$ and $30 \mu\text{m}$ wide and $h = 25 \mu\text{m}$ tall microridges aligned parallel to the flow direction. The spacing between the microridges was varied from $w = 20$ to $120 \mu\text{m}$ and the microchannel height was varied from $H = 76.2$ to $254 \mu\text{m}$ while keeping the aspect ratio fixed at $\alpha = 20$. Although the height of the microridges in our experiments were fixed at $h = 25 \mu\text{m}$, we showed in our previous work through laser confocal metrology measurements that even under the largest pressure drops we could apply across our microchannels, the air-water interface does not deflect more than a few micrometers.⁹ Therefore, for most applications, microridges with heights no more than a few micrometers are needed to insure that the air-water interface does not come into contact with the base of the valley between the microposts. At these depths the pressure drop reduction achieved through the use of these ultrahydrophobic surfaces (15%–25% for channel depths between 250 and $75 \mu\text{m}$) outweighs the benefits from say simply expanding the channel by an additional $4 \mu\text{m}$ (3%–12% improvement over the same range).⁹ Clearly, these surfaces are most advantageous for larger microchannels where small increases in the channel size do not result in significant reduction in the pressure drop or even as a surface treatment for objects in an external flow.

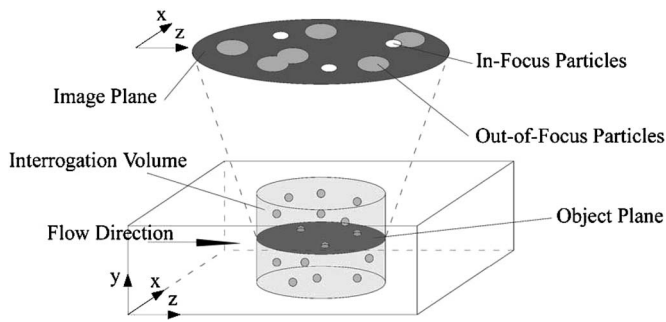


FIG. 4. Schematic diagram demonstrating how out-of-focus particles can appear on the image plane when using an epifluorescence microscope for μ -PIV.

C. Microparticle image velocimetry (μ -PIV)

To probe the velocity fields near the micropatterned surfaces and the existence of slip, detailed velocity measurements of the flow field were made using microparticle image velocimetry (μ -PIV) technique developed by Santiago *et al.*^{23,28} For channels with significantly larger gaps ($H \gg 1$ mm) standard digital particle image velocimetry (PIV) technique^{29,30} would have been possible. However, in order to resolve the flow kinematics at and below the lengthscales of the surface topology μ -PIV was required.

The μ -PIV technique was implemented using an epifluorescent microscope (Zeiss 200 M, Oregon, USA) to make velocity profile measurements of the flow past the ultrahydrophobic surfaces. The distilled, de-ionized water was seeded with fluorescently tagged Nile red aliphatic latex spheres 1 μm in diameter (6-NF-1000, Interfacial Dynamics Corp.). The fluorescent particles were chosen to absorb the green incident laser light and emit red light. The emission from the tracer particles was collected an intensified CCD camera (N50, HAMAMATSU, Japan) at 30 fps. As with standard PIV techniques, successive images were captured with a given delay time and the flow velocities were calculated by correlating particle displacement using a PIV algorithm successfully implemented in the past.^{30–32} In order to account for the short (180 μm) working distance of the microscope, the glass cover slip on the flow cell used to take pressure drop measurement was replaced with a significantly thinner microscope cover slip (#0, Electron Microscopy Sciences, Pennsylvania, USA). Thinner microchannels were also required to make velocity measurement possible across the entire channel. For all the μ -PIV experiments presented in this manuscript, the channel depth was held fixed at $H=85$ μm .

One of the difficulties associated with using an epifluorescent microscope to take μ -PIV measurements is that the excitation light exposes particles within a volume of fluid as opposed to the a plane of fluid typically exposed by standard PIV techniques.³³ This can be seen schematically in Fig. 4. The particles within the interrogation volume will fluoresce simultaneously making it difficult to achieve good spatial resolution in the PIV measurements normal to the plane of the ultrahydrophobic surface (z direction). The in-focus particles will appear as sharp, bright points, while the out-of-

focus particles will appear as either larger, discrete points or a background glow. To minimize the effect of out-of-focus particles and therefore the variation of the particle velocity across the focal plane, a high numerical aperture oil-immersion objective (100 \times /1.3 Oil, Zeiss) with 100 \times magnification was used. The depth of field for the lens can be calculated by the standard formula for a microscope objective lens³⁴

$$\delta z = \frac{n\lambda_0}{NA^2} + \frac{ne}{NAM} = 0.58 \mu\text{m}. \quad (2)$$

Here n is the refractive index of the fluid between the objective lens and the cover slip, NA is the numerical aperture of the objective lens, λ_0 is the wavelength of the excitation light source, e is the smallest distance that can be resolved on the detector or a single pixel of a charge coupled device (CCD) camera, and M is the total magnification of the system. Meinhart *et al.*³⁵ showed that when making μ -PIV measurements it is not the depth of field, but the measurement depth which sets the resolution of the μ -PIV measurements. The measurement depth is defined as twice the distance from the center of the object plane to the point beyond which the intensity of the particle image has been reduced to the point that it no longer influences the velocity measurement

$$\delta z_m = \frac{3n\lambda_0}{NA^2} + \frac{2.16d_p}{\tan \theta} + d_p. \quad (3)$$

Here d_p is the diameter of the seed particles and θ is the light collection angle. In our experiments the depth of measurement is approximately $\delta z_m=5.28$ μm . To further reduce the effect of out-of-focus particles, a threshold was applied to each image before correlation to remove the glow of the far out-of-focus particles. The resulting image plane had dimensions of 85 $\mu\text{m} \times 64$ μm making it possible to fully resolve the flow over several microridges and the air-water interface supported between them.

The fluorescently tagged microspheres were chosen such that they were small enough to move affinely with the fluid without disturbing the flow and large enough that they could be easily observable within the flow. Following the experiments of Santiago *et al.*,^{23,28} the μ -PIV measurements were performed using commercially available 1.0 μm diameter polystyrene spheres. At these small scales, the path of the seed particles is influenced by Brownian/thermal motion, however, because the flow is steady, it is possible to eliminate this random noise by averaging a large number of velocity correlations together to produce a single velocity vector field.³⁶ To illustrate the effectiveness of this technique, a series of velocity measurements are presented in Fig. 5. In Fig. 5(a), an image of the fluorescing tracer particles is shown. In this image, the microscope was focused 25 μm away from an ultrahydrophobic surface patterned with $w=30$ μm wide microridges spaced $d=30$ μm apart and under a water flow rate of $Q=0.001$ ml/s. The location of the image was positioned 5 mm downstream of the channel inlet to insure the flow was fully developed. Notice the variation of size and brightness of the particles in the image as well the less-than-optimal particle density. The velocity vector field

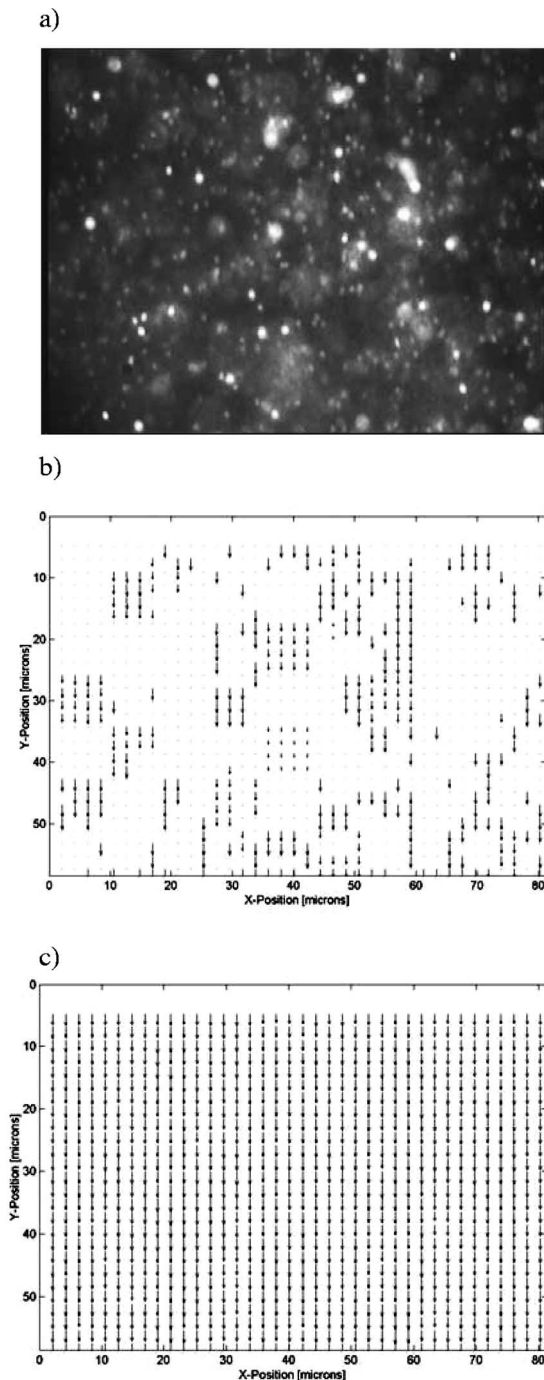


FIG. 5. Demonstration of μ -PIV technique. (a) Image of fluorescent seed particles in flow; (b) velocity profile produced by the correlation of two images; and (c) velocity profile produced by averaging the velocities from 100 correlations. In (b) and (c), an arrow with a length equal to $10\ \mu\text{m}$ corresponds to a velocity of $70\ \mu\text{m/s}$.

shown in Fig. 5(b) was calculated by using a standard PIV technique to correlate the image in Fig. 5(a) with a second image acquired $1/30$ th second later. The variation of the magnitude and direction of the velocity vectors is the result of Brownian fluctuations whereas the lack of viable velocity vectors in many subcorrelation windows [denoted by dots in Fig. 5(b)] is the result of low particle density. By averaging over a series of 100 velocity correlations, a more complete and a significantly less noisy velocity profile can be gener-

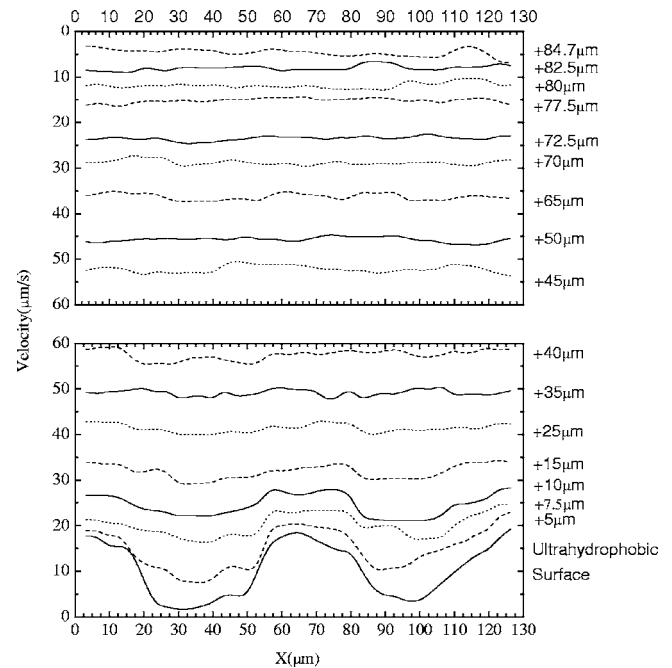


FIG. 6. μ -PIV measurements of the velocity profile at different depths across an $H=85\ \mu\text{m}$ tall microchannel. The bottom surface ($z=0$) is an ultrahydrophobic surface containing $w=30\ \mu\text{m}$ wide microridges spaced $d=30\ \mu\text{m}$ apart.

ated while simultaneously gathering statistical information such as the standard deviation. The final velocity vector field is shown in Fig. 5(c).

As shown schematically in Fig. 4, the images and therefore the velocity vector fields acquired through μ -PIV, are for the flow in the xz plane. In order to build up a fully three-dimensional velocity vector field, the focal plane of the epifluorescent microscope was moved vertically through the microchannel from the ultrahydrophobic surface to the glass cover slip. Velocity measurements were taken at a series of different depths within the microchannel and used to build up the velocity profile in the xz plane.

III. RESULTS AND DISCUSSION

A series of experiments were performed to measure the detailed kinematics for the flow over ultrahydrophobic surfaces and to obtain a more complete understanding of the ultrahydrophobic drag reduction mechanism. The effects of channel height, microridge spacing, and size were systematically investigated. In Fig. 6, a series of velocity profiles are presented at various depths within the microchannel. For this experiment an ultrahydrophobic surface with $d=30\ \mu\text{m}$ wide microridges set $w=30\ \mu\text{m}$ apart was used as the microchannel's top surface. The bottom surface of the microchannel was a glass cover slip which allowed the motion of the fluorescent seed particles to be captured by an epifluorescent microscope. With $1000\times$ total magnification, the images captured by the CCD camera spanned $85\ \mu\text{m}$, which makes it possible to simultaneously measure the flow kinematics over two complete microridges and the shear-free air-water interface supported between them.

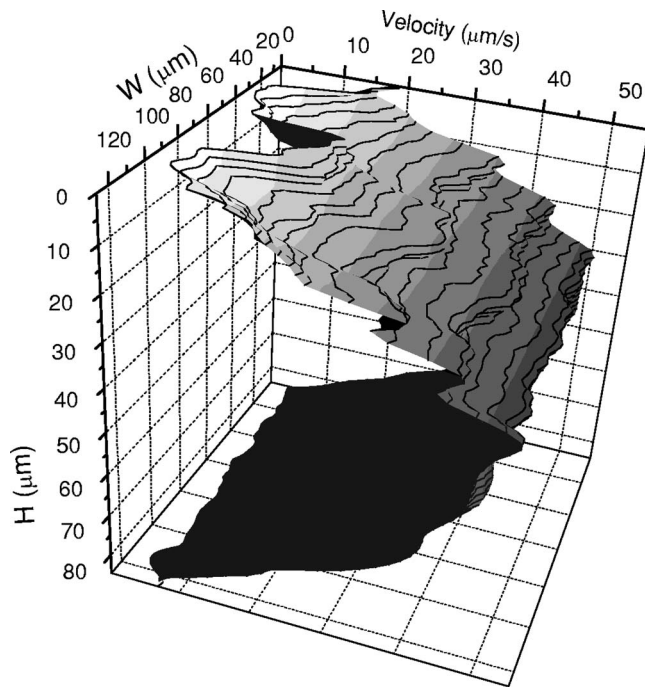


FIG. 7. Velocity profile in the xy plane generated from the μ -PIV measurement presented in Fig. 6.

The velocity measurements very near to the ultrahydrophobic surface show a slip velocity that is near zero along the span of each microridge. As one moves from the edge of the microridge and proceeds across the air-water interface, the slip velocity increases and reaches a maximum of nearly $20 \mu\text{m/s}$ at the center of the interface. This slip velocity corresponds to roughly 50% of the average velocity in the microchannel. The velocity profile is periodic from one microridge to the next. As the measurement plane is moved away from the ultrahydrophobic surface, the influence of the surface slip velocity was found to decay relatively quickly. The influence of the shear-free air-water interface was found to persist into the microchannel a distance roughly 20% of the channel height. The no-slip velocity profile is again nearly recovered on the glass cover slide. The slightly non-zero velocity measured along the glass cover slip and the no-slip microridge is a result of the finite depth of field of the microscope objective. The velocity measurements represent an average velocity of all the particles flowing through the interrogation window. In addition, an uncertainty equal to plus or minus one half the measurement depth, $\pm 0.5\delta z_m$, exists in the absolute position of the measurement plane.

In Fig. 7, the velocity vector fields measured within the xz -plane are stacked to build up a three-dimensional representation of the velocity profile across the microchannel in the xy plane. These detailed μ -PIV measurements represent the first direct measurements of slip over ultrahydrophobic surfaces. By resolving the flow below the length scale of the periodic microridge surface structure, the velocity measurements clearly demonstrate that the shear-free air-water interface supported between the hydrophobic micrometer-sized ridges is the primary physical mechanism responsible for the pressure drop reduction observed for flows over ultrahydro-

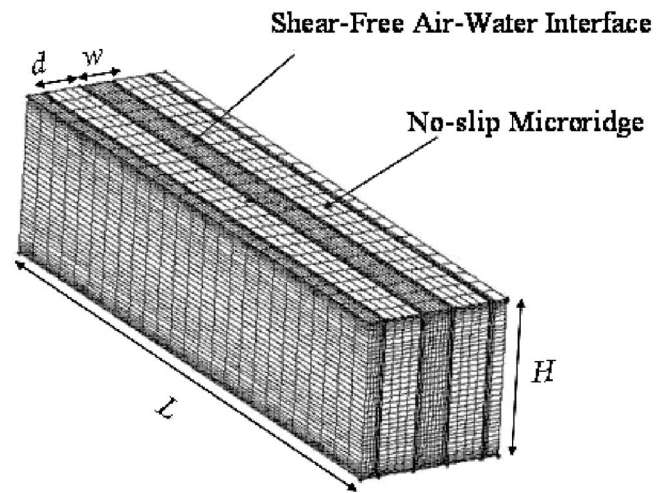


FIG. 8. An example of one of the meshes used for the numerical simulations of flow past ultrahydrophobic surface containing bands of no-slip microridges and shear free. The top surface which is not shown here is also no-slip whereas periodic boundary conditions were used for the side walls.

phobic surfaces. The reduction in effective contact area between the fluid and the solid surface allows the fluid to flow with significantly less resistance. To further evaluate the model of ultrahydrophobic drag reduction, a series of numerical simulations were performed and compared directly to the experimental measurements.

The channel flow was modeled using the computation fluid dynamics (CFD) package FluentTM (Fluent Inc., New Hampshire, USA). An example of the mesh that was used to perform these simulations is shown in Fig. 8. Three microridges were included in the flow domain and periodic boundary conditions were assumed in both the streamwise and the spanwise directions. A systematic study was performed to insure that the simulations had adequate resolution to resolve the necessary physics and were not sensitive to further mesh refinement. The numerical simulations assumed no deflection of the free surface and treated the air-water interface as a solid shear-free surface. This assumption is valid for large surface tension, small spacing between posts or low pressures. However, as Ou *et al.*⁹ demonstrated, the free surface can deflect by several micrometers under flow conditions. It should be noted, however, that to perform the μ -PIV measurements described previously, the flow rates applied and therefore the pressure drop produced were extremely small and minimal free surface deflection is expected.

The velocity profile across a microchannel $127 \mu\text{m}$ high, $500 \mu\text{m}$ long, and contained two $30 \mu\text{m}$ wide microridges set $30 \mu\text{m}$ apart was calculated and is presented in Fig. 9. The geometry was chosen such that a direct comparison could be made between these numerical simulations and the experimental velocity profile measurements in Fig. 6. As defined by the boundary conditions, the velocity along the no-slip microridges is zero. Above the microridge the velocity increases to a maximum near the center line and returns to zero at the opposite wall. The velocity along the shear-free air-water interface varies smoothly from zero at the edge of the microridge to a maximum slip velocity at the center of the shear-free band. For the particular geometry, the slip ve-

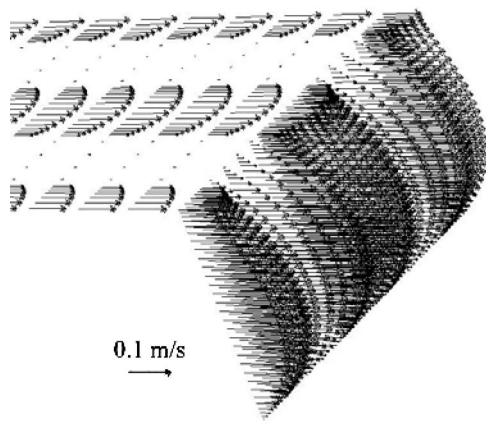


FIG. 9. Velocity profile obtained from the numerical simulation of flow through an $H=85\ \mu\text{m}$ tall microchannel at an average velocity of $U=0.1\ \text{m/s}$ past a model ultrahydrophobic surface containing $w=30\ \mu\text{m}$ wide microridges spaced $d=30\ \mu\text{m}$ apart.

locity of the fluid along the shear-free band reaches a maximum velocity of approximately one half the average velocity in the channel, $u_{z,0}=0.51U$. If the average velocity along the model ultrahydrophobic surface is calculated, the average slip velocity becomes $\bar{u}_{z,0}=0.17U$ which corresponds to a slip length of $b=7.5\ \mu\text{m}$. This compares well to the slip length of $b=5.0\ \mu\text{m}$ calculated indirectly from the experimental pressure drop measurement.⁹

The CFD velocity field in Fig. 9 is in good qualitative agreement with the experimental μ -PIV measurements in Fig. 7. However, to obtain a more quantitative comparison between experiments and numerical simulations, the velocity profile across a vertical slice (y direction) through the center of a microridge and the center of the shear-free air-water interface are shown in Fig. 10. The agreement between the experimental μ -PIV measurements and the numerical simulations is quite good resulting in a quantitative agreement within experimental error across the entire microchannel. Note that beyond a dimensionless channel depth of $y/H > 0.2$, the influence of the air-water interface is no longer observable and the velocity profiles above the microridge and the interface become indistinguishable. In addition, the velocity profile very near the air-water interface shows a dramatically reduced velocity gradient and therefore a significantly reduced shear stress. These measurements clearly demonstrated the kinematical origins of drag reduction over ultrahydrophobic surfaces.

The error bars on the velocity are calculated as the standard deviation of the velocity calculated from 100 μ -PIV correlations. The error bars on the channel position correspond to the error in locating the particle position due to depth of field and the presence of out of focus particles. A pattern of the ultrahydrophobic surface with a larger dimensionless microridges spacing, $d=30\ \mu\text{m}$ and $w=60\ \mu\text{m}$, was also test. The results of the μ -PIV measurements and the numerical simulations for the velocity profile above the shear-free air-water interface are superimposed over the $w=30\ \mu\text{m}$ data in Fig. 10. A quantitative fit is again achieved between the μ -PIV measurement and the predictions of the numerical simulations. By increasing the spacing between

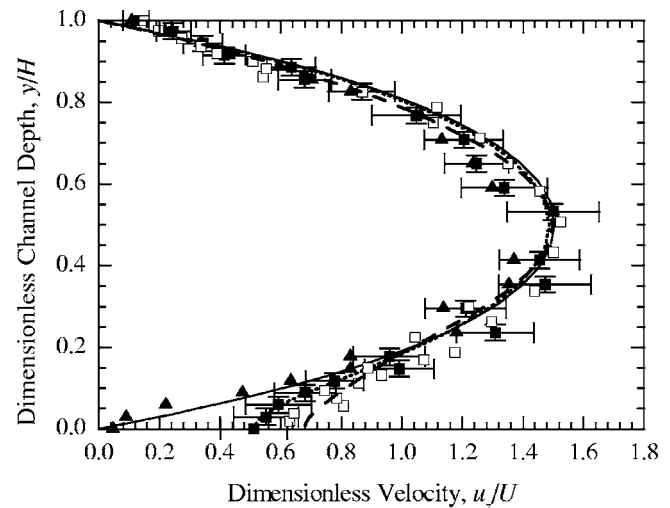


FIG. 10. Direct comparison of the velocity profiles measured through μ -PIV and predicted from numerical simulations for the flow through an $H=85\ \mu\text{m}$ tall microchannel past a series of ultrahydrophobic surfaces contain $w=30\ \mu\text{m}$ wide microridges spaced $d=30\ \mu\text{m}$ (solid symbols) and $d=60\ \mu\text{m}$ (open symbols) apart. The data include μ -PIV measurement include the velocity profile for a vertical slice taken above the center of microridge (\blacktriangle), above the center of $30\ \mu\text{m}$ shear-free interface (\blacksquare), above the center of $60\ \mu\text{m}$ shear-free interface (\square), and the corresponding numerical simulations.

the microposts, the maximum slip velocity across the air-water interface was found to increase by 20% to $u_{z,0}=0.63U$. The increase in slip velocity corresponds to an increase in slip length and a corresponding increase in the pressure drop reduction with increased microridge separation.⁹ However, even with an increased microridge spacing, the influence of the air-water interface does not extend significantly further into the flow. The velocity profiles above the microridge and the interface again become nearly indistinguishable beyond a dimensionless channel depth of $y/H > 0.2$.

With the quantitative agreement between the numerical simulations and the detailed experimental velocity measurements, the numerical simulations become a powerful tool for evaluating and optimizing the drag reduction for flow over ultrahydrophobic surfaces; whether the surfaces contains a periodic series of microridges, microposts or some other novel microstructure. To further investigate the effectiveness of the numerical simulations as a design tool, the flow past a series of ultrahydrophobic surfaces containing microridges $d=20$ and $30\ \mu\text{m}$ wide, spaced $w=20$ and $30\ \mu\text{m}$ apart, respectively, and standing $h=30\ \mu\text{m}$ tall were examined both experimentally and numerically for a series of rectangular microchannel with channel heights varying from $H=76.2\ \mu\text{m}$ to $254\ \mu\text{m}$ and having a fixed aspect ratio of $\alpha=20$. These particular ultrahydrophobic surfaces were chosen to investigate the role of the microridge size on the pressure drop reduction while holding the dimensionless microridge spacing fixed at $\beta=w/(d+w)=0.50$. The dimensionless microridge spacing is equivalent to the ratio of area of the shear-free air-water interface supported by the microridges to total area of the surface.

For both ultrahydrophobic surfaces examined, the pres-

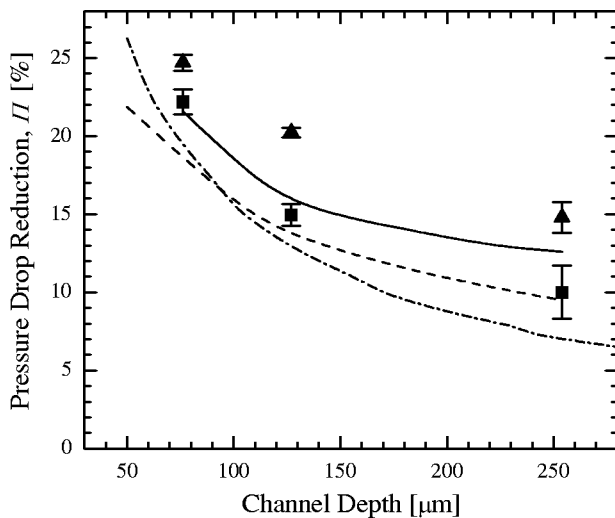


FIG. 11. Pressure drop reduction as a function of channel depth for the flow through a microchannel with an aspect ratio of $\alpha=20$ and a length of $L=50$ mm past an ultrahydrophobic surface with $d=20$ μm wide microridges spaced $w=20$ μm apart (\blacksquare) and $d=30$ μm wide microridges spaced $w=30$ μm apart (\blacktriangle). Also included is the prediction of the analytical solution of Philip (Refs. 10 and 11) for $d=30$ μm wide microridges spaced $w=30$ μm apart (---), and the result of numerical simulation of $d=20$ μm wide microridges spaced $w=20$ μm apart (- -) and $d=30$ μm wide microridges spaced $w=30$ μm apart (—).

sure drop reduction was found to decrease with increasing channel height. However, even though each of the ultrahydrophobic surface tested contained the same percentage of shear-free air-water interface, increasing the spacing of the microridges from 20 to 30 μm resulted in a significant increase in the pressure drop reduction. Further, the percent increase in the pressure drop reduction with increasing microridge width appears to increase with increasing channel depth. These observations are physically intuitive. Consider a hypothetical surface where, like the surfaces in Fig. 11, the dimensionless microridge spacing is fixed at $\beta=0.5$, but where the width of the microridges and their spacing approaches zero. Even though the microridges support the same amount of shear-free air-water interface, the slip velocity on the free interface and therefore the pressure drop reduction will approach zero as the spacing between the microridges goes to zero. This suggests that there is a lower bound in microridge spacing for which significant pressure drop reduction can be achieved.

A series of numerical simulations were performed for the same ultrahydrophobic surfaces designs and spanning the same range of microchannel heights. The results of the numerical simulations are superimposed over the experimental data in Fig. 11. The numerical simulations are in qualitative agreement with the results of the experiments; however, the numerical simulations systematically underpredict the pressure drop reduction. Unlike the μ -PIV experiments which were performed at extremely small volume flow rates and pressure drops, the pressure drop measurements were taken at flow rates large enough to produce a modest (~ 1 – 2 μm) deflection in the air-water interface. This deflection would produce an additional pressure drop reduction that is unaccounted for in the numerical simulations by ef-

fectively increasing the cross sectional area of the microchannel. Molecular dynamics simulations have shown that the deflection of the air-water interface between hydrophobic microridges can result in a decrease of the slip length as compared to continuum simulations with a flat shear-free air-water interface.^{37,38} However, this dissipative effect appears to be a result of the molecular lengthscales used in the molecular dynamics simulations.³⁹ To investigate the role of free surface curvature further, a series of numerical simulations were performed with arbitrary deflections of 1–5 μm imposed upon the air-water interface. In all cases, the deflection of the interface resulted in an increase of the pressure drop reduction and slip length predicted by the numerical simulations bringing the predictions of the numerical simulations more in-line with the experimental measurements.

The experimental results and numerical simulations can also be compared to the analytical solutions of Philip.^{10,11} Philip derived an analytical solution to Stokes flow in an infinite channel where one wall is no-slip whereas the other wall contains a periodic array of shear-free bands running parallel to the flow direction. Philip showed that the velocity profile across the gap became

$$u_z(x,y) = \frac{H^2}{2\mu} \left(-\frac{\partial p}{\partial z} \right) \left\{ \frac{y}{H} \left(1 - \frac{y}{H} \right) + \text{Im} \left[\frac{1}{K'(k_1)} c_n^{-1} \left(\frac{c_n \left(K(k) \frac{x+iy}{(w+d)}, k \right)}{c_n \left(K(k) \frac{w}{(w+d)}, k \right)} \right) - \frac{x+iy}{H} \right] \right\}. \quad (4)$$

where k is defined by $K'(k)/K(k)=2H/(w+d)$ and $k_1=kc_d[K(k)w/(w+d),k]$. Here K and K' are the complete elliptic integrals and c_d and c_n are the Jacobian elliptic functions. Although, difficulties associated with evaluating the inverse Jacobian elliptic function of a complex number rendered it impossible to evaluate Philip's prediction of the velocity profile for our geometries, by integrating Eq. (4) across the channel, a tractable expression for the volume flow rate can be calculated. Philip¹¹ showed that for a given pressure drop, the addition of the shear-free bands results in an increase in the volume flow rate per $(w+d)/2$ strip of ultrahydrophobic surface of

$$\Delta q = \frac{(w+d)H^3}{12\mu} \left(-\frac{\partial p}{\partial z} \right) \left(3 - \frac{3wB_1}{(w+d)} \right). \quad (5)$$

Equation (5) can also be made dimensionless by dividing by the volume flow rate for the flow between two no-slip plates, $\Delta q/q_{\text{no-slip}}=3[1-wB_1/(w+d)]$. Here Philip defines

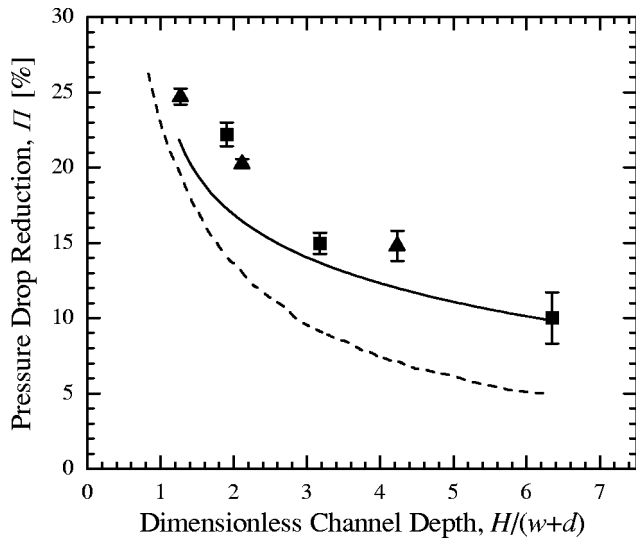


FIG. 12. The pressure drop reduction data from Fig. 11 recast as pressure drop reduction as a function of dimensionless channel depth, $\gamma=H/d$. The data for the flow past ultrahydrophobic surfaces with $d=20\ \mu\text{m}$ wide microridges spaced $w=20\ \mu\text{m}$ apart (■) and $d=30\ \mu\text{m}$ and $w=30\ \mu\text{m}$ (▲) collapse onto a single master curve. The numerical simulation of (—) and Philip solution (Refs. 10 and 11) (---) for both $d=20\ \mu\text{m}$ and $w=20\ \mu\text{m}$ and $d=30\ \mu\text{m}$ and $w=30\ \mu\text{m}$ are also shown to collapse.

$$B_1 = \frac{K'(k_1)}{K(k_1)} \frac{2H}{(w+d)}. \quad (6)$$

The predictions of the Philip model are superimposed over the experimental pressure drop reduction data and predictions of the numerical simulations in Fig. 11. Like the numerical simulations, the Philip model qualitatively captures the trend in the data, but systematically underpredicts the magnitude of the pressure drop reduction. As described above, the discrepancies between the predictions of the analytical theory and the experimental measurements most likely originate from the slight deflection in the air-water interface present in the experiments.

The Philip model predicts that the pressure drop reduction is a function of both the dimensionless microridge separation and the dimensionless channel depth, $\Pi=f[w/(w+d), H/(w+d)]$. The Philip model, therefore, suggests that the influence of microridge width on the pressure drop reduction could be eliminated if the data in Fig. 11 were recast as a function of the dimensionless channel depth, $\delta=H/(w+d)$. Indeed, the pressure drop reduction data do collapse onto a single master curve as shown in Fig. 12 and appears to have a $\Pi \propto \delta^{-1/2}=[H/(w+d)]^{-1/2}$ dependence, although from Eqs. (5) and (6), this scaling is more complicated than a simple power law. For large dimensionless channel depths, our previous experimental measurements⁹ suggest that when the channel depth is held fixed, the pressure drop reduction grows roughly as the dimensionless micropost spacing squared, $\Pi \propto [w/(w+d)]^2$. Starting from Eq. (1), the pressure drop reduction can be expressed in terms of the slip length $\Pi=3b/(4b+H)$. In the limit of large b , the pressure drop reduction approaches $\Pi \rightarrow 0.75$. This limit is recovered by the predictions of the Philip model. In the limit that $b \ll H$, the dimensionless slip length b/H will follow the

same scaling as the dimensionless pressure drop and be a function of both the width of the air-water interface and channel height. The agreement between the predictions of the Philip model, the numerical simulations and the experimental results, provides further confirmation that the existence of slip along the shear-free air-water interface between microprotrusions is the correct physical model for interpreting the observed drag reduction past ultrahydrophobic surfaces.

IV. CONCLUSIONS

In this article, we have shown through a carefully designed set of experiments and numerical simulations that the shear-free air-water interface supported between peaks of micrometer-sized roughness is the primary physical cause of drag reduction in flows past ultrahydrophobic surfaces. A microchannel was used to take pressure drop and μ -PIV measurement of the flow past a series of ultrahydrophobic silicon surfaces patterned with 20 and 30 μm wide microridges spaced between 20 and 120 μm apart using standard photolithographic techniques. An increase in pressure drop reduction with increasing microridge spacing and decreasing channel depth was observed. Experiments showed that for a fixed percentage of shear-free air-water interface, the pressure drop reduction decreases with decreasing microridge spacing. This observation suggests that there is a minimum microridge spacing below which significant drag reduction cannot be achieved even if a significant amount of shear-free interface can be produced.

μ -PIV measurements were used to systematically and precisely probe the detailed flow kinematics throughout the microchannel at lengthscales well below that of the surface roughness. Velocity measurements were made above both the microridges and the air-water interface supported between the microridges. Although the flow along the microridges was found to be no-slip, slip velocities greater than 60% the average velocity were measured along the air-water interface. These measurements demonstrate a direct correlation between the increase in the pressure drop reduction and the increase in the slip velocity along the shear-free air-water interface.

A series of numerical simulations were performed to further test the validity of the ultrahydrophobic drag reduction model. The microridges were modeled as a series of solid no-slip and shear-free bands. The predictions of the numerical simulations were found to quantitatively fit the experimental velocity data within experimental error and qualitatively fit the experimental pressure drop reduction data. These results, thus, provide further proof that ultrahydrophobic drag reduction is due to the existence of a shear-free air-water interface between microprotrusions which results in a reduced effective contact area between the fluid and the solid surface.

ACKNOWLEDGMENTS

The authors would like to thank Anthony Dinsmore of the University of Massachusetts for the use of his epifluores-

cent microscope. This research was partially supported by a Healey Endowment Grant and 3M through a Non-Tenured Faculty Award. The authors would also like to thank the referees for their comments and suggestions.

- ¹W. Barthlott and C. Neinhuis, "Purity of the sacred lotus, or escape from contamination in biological surfaces," *Planta* **202**, 1 (1997).
- ²D. Oner and T. J. McCarthy, "Ultrahydrophobic surfaces. Effects of topography length scales on wettability," *Langmuir* **16**, 7777 (2000).
- ³J. Bico, C. Marzolin, and D. Quere, "Pearl drops," *Europhys. Lett.* **47**, 220 (1999).
- ⁴J. P. Youngblood and T. J. McCarthy, "Ultrahydrophobic polymer surfaces prepared by simultaneous ablation of polypropylene and sputtering of poly(tetrafluorethylene) using radio frequency plasma," *Macromolecules* **32**, 6800 (1999).
- ⁵A. Y. Fadeev and T. J. McCarthy, "Trialkylsilane monolayers covalently attached to silicon surfaces: Wettability studies indicating that molecular topography contributes to contact angle hysteresis," *Langmuir* **15**, 3759 (1999).
- ⁶W. Chen, A. Y. Fadeev, M. C. Hsieh, D. Oner, J. P. Youngblood, and T. J. McCarthy, "Ultrahydrophobic and ultralyophobic surfaces: Some comments and examples," *Langmuir* **15**, 3395 (1999).
- ⁷A. Nakajima, K. Hashimoto, and T. Watanabe, "Recent studies on superhydrophobic films," *Monatsh. Chem.* **132**, 31 (2001).
- ⁸J. Kim and C.-J. Kim, in *IEEE Conference MEMS* (Las Vegas, NV, 2002), p. 479.
- ⁹J. Ou, J. B. Perot, and J. P. Rothstein, "Laminar drag reduction in microchannels using ultrahydrophobic surfaces," *Phys. Fluids* **16**, 4635 (2004).
- ¹⁰J. R. Philip, "Flows satisfying mixed no-slip and no-shear conditions," *Z. Angew. Math. Phys.* **23**, 353 (1972).
- ¹¹J. R. Philip, "Integral properties of flows satisfying mixed no-slip and no-shear conditions," *Z. Angew. Math. Phys.* **23**, 960 (1972).
- ¹²E. Lauga and H. A. Stone, "Effective slip in pressure driven Stokes flow," *J. Fluid Mech.* **489**, 55 (2003).
- ¹³S. Goldstein and Aeronautical Research Council (Great Britain, *Modern Developments in Fluid Dynamics; an Account of Theory and Experiment Relating to Boundary Layers, Turbulent Motion and Wakes* (Dover, New York, 1965).
- ¹⁴Y. Zhu and S. Granick, "Limits of hydrodynamic no-slip boundary conditions," *Phys. Rev. Lett.* **88**, 106102 (2002).
- ¹⁵Y. Zhu and S. Granick, "Rate-dependent slip of Newtonian liquids at smooth surfaces," *Phys. Rev. Lett.* **87**, 096105 (2001).
- ¹⁶E. Schnell, "Slippage of water over nonwetttable surfaces," *J. Appl. Phys.* **27**, 1149 (1956).
- ¹⁷J.-L. Barrat and L. Bocquet, "Large slip effect at a nonwetting fluid-solid interface," *Phys. Rev. Lett.* **82**, 4671 (1999).
- ¹⁸J. Baudry, E. Charlaix, A. Tonck, and D. Mazuyer, "Experimental evidence for a large slip effect at a nonwetting fluid-surface interface," *Langmuir* **17**, 5232 (2001).
- ¹⁹D. C. Tretheway and C. D. Meinhart, "Apparent fluid slip at hydrophobic microchannel walls," *Phys. Fluids* **14**, L9 (2002).
- ²⁰D. C. Tretheway and C. D. Meinhart, "A generating mechanism for apparent fluid slip in hydrophobic microchannels," *Phys. Fluids* **16**, 1509 (2004).
- ²¹R. Pit, H. Hervet, and L. Leger, "Friction and slip of a simple liquid at a solid surface," *Tribol. Lett.* **7**, 147 (1999).
- ²²S. Jin, P. Huang, J. Park, J. Y. Yoo, and K. S. Breuer, "Near-surface velocity using evanescent wave illumination," *Exp. Fluids* **37**, 825 (2004).
- ²³C. D. Meinhart, S. T. Wereley, and J. G. Santiago, "PIV measurements of a microchannel flow," *Exp. Fluids* **27**, 414 (1999).
- ²⁴K. Watanabe, H. Yanuar, and H. Udagawa, "Drag reduction of Newtonian fluid in a circular pipe with highly water-repellent wall," *J. Fluid Mech.* **381**, 225 (1999).
- ²⁵K. Watanabe, T. Takayama, S. Ogata, and S. Isozaki, "Flow between two coaxial rotating cylinders with a highly water-repellent wall," *AIChE J.* **49**, 1956 (2003).
- ²⁶F. M. White, *Fluid Mechanics* (McGraw-Hill, New York, 2003).
- ²⁷J. C. McDonald, D. C. Duffy, J. R. Anderson, D. T. Chiu, O. J. A. Schueler, and G. M. Whitesides, "Fabrication of microfluidic systems in poly(dimethylsiloxane)," *Electrophoresis* **21**, 27 (2000).
- ²⁸S. Devasenathipathy, J. G. Santiago, S. T. Wereley, C. D. Meinhart, and K. Takehara, "A particle image velocimetry system for microfluidics," *Exp. Fluids* **25**, 316 (1998).
- ²⁹R. J. Adrian, "Particle-imaging techniques for experimental fluid mechanics," *Annu. Rev. Fluid Mech.* **23**, 261 (1991).
- ³⁰J. P. Rothstein and G. H. McKinley, "The axisymmetric contraction-expansion: The role of extensional rheology on vortex growth dynamics and the enhanced pressure drop," *J. Non-Newtonian Fluid Mech.* **98**, 33 (2001).
- ³¹S. Chen and J. P. Rothstein, "Flow of a wormlike micelle solution past a falling sphere," *J. Non-Newtonian Fluid Mech.* **116**, 205 (2004).
- ³²D. Hart, "High-speed PIV analysis using compressed image correlation," *J. Fluids Eng.* **120**, 463 (1998).
- ³³M. G. Olsen and R. J. Adrian, "Out of focus effects on particle image visibility and correlation in microscopic particle image velocimetry," *Exp. Fluids* **29**, S166 (2000).
- ³⁴S. Inoue, *Video Microscopy* (Plenum, New York, 1986).
- ³⁵C. D. Meinhart, S. T. Wereley, and M. H. B. Gray, "Volume illumination for two-dimensional particle image velocimetry," *Meas. Sci. Technol.* **11**, 809 (2000).
- ³⁶C. D. Meinhart, S. T. Wereley, and J. G. Santiago, "A PIV algorithm for estimating time-averaged velocity fields," *J. Fluids Eng.* **122**, 285 (2000).
- ³⁷C. Cottin-Bizonne, C. Barentin, E. Charlaix, L. Bocquet, and J.-L. Barrat, "Dynamics of simple liquids at heterogeneous surfaces: Molecular dynamics simulations and hydrodynamic description," *Eur. Phys. J. E* **15**, 427 (2004).
- ³⁸C. Cottin-Bizonne, J.-L. Barrat, L. Bocquet, and E. Charlaix, "Low-friction flows of liquid at nanopatterned interfaces," *Meteorit. Planet. Sci.* **38**, 237 (2003).
- ³⁹N. V. Priezjev, A. A. Darhuber, and S. M. Troian, "Slip behavior in liquid films on surfaces of patterned wettability: Comparison between continuum and molecular dynamics simulations," *Phys. Rev. E* **71**, 041608 (2005).